

# Fast and Accurate Unknown Object Instance Segmentation through Error-Informed Refinement

Seunghyeok Back, Sangbeom Lee, Kangmin Kim, Joosoon Lee, Sungho Shin, Jemo Maeng, and Kyoobin Lee

**Abstract**—Accurate perception of unknown objects is essential for autonomous robots, particularly when manipulating novel items in unstructured environments. However, existing unknown object instance segmentation (UOIS) methods often have over-segmentation and under-segmentation problems, resulting in inaccurate instance boundaries and failures in subsequent robotic tasks such as grasping and placement. To address this challenge, this article introduces INSTA-BEER, a fast and accurate model-agnostic refinement method that enhances the UOIS performance. The model adopts an error-informed refinement approach, which first predicts pixel-wise errors in the initial segmentation and then refines the segmentation guided by these error estimates. We introduce the quad-metric boundary error, which quantifies pixel-wise true positives, true negatives, false positives, and false negatives at the boundaries of object instances, effectively capturing both fine-grained and instance-level segmentation errors. Additionally, the Error Guidance Fusion (EGF) module explicitly integrates error information into the refinement process, further improving segmentation quality. In comprehensive evaluations conducted on three widely used benchmark datasets, INSTA-BEER outperformed state-of-the-art models in both accuracy and inference time. Moreover, a real-world robotic experiment demonstrated the practical applicability of our method in improving the performance of target object grasping tasks in cluttered environments.

**Index Terms**—Error-informed refinement, robotic grasping, segmentation refinement, unknown object instance segmentation

## I. INTRODUCTION

Segmenting unknown objects is a fundamental skill for robots to perceive and manipulate novel objects in unstructured environments effectively. Intelligent robotic systems are required to detect and identify objects accurately, even when encountering novel objects in cluttered scenes. Recently, unknown object instance segmentation (UOIS) [1]–[3] has emerged as a key task for enabling robots to interact with novel objects in complex environments. UOIS aims to segment all object instances in a category-agnostic manner, where test objects and environments are unknown and not previously encountered during training. State-of-the-art UOIS methods

This work was fully supported by the Korea Institute for Advancement of Technology (KIAT) grant funded by the Korea Government (MOTIE) (Project Number: 20008613). This work was partially supported by Artificial intelligence industrial convergence cluster development project funded by the Ministry of Science and ICT (MSIT, Korea) & Gwangju Metropolitan City. (Corresponding author: Kyoobin Lee)

All authors are with the School of Integrated Technology (SIT), Gwangju Institute of Science and Technology (GIST), Cheomdan-gwagiro 123, Buk-gu, Gwangju 61005, Republic of Korea. (e-mail: shback@gm.gist.ac.kr, sat-urnbeom@gm.gist.ac.kr, kgmin156@gm.gist.ac.kr, joosoon1111@gist.ac.kr, hogjili89@gm.gist.ac.kr, maengjemo@gm.gist.ac.kr, kyoobinlee@gist.ac.kr) The project website is <https://sites.google.com/view/insta-beer>.

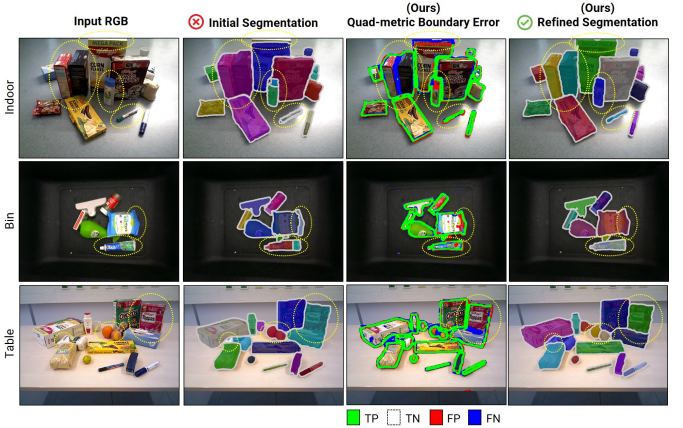


Fig. 1. Effective refinement of unknown object instance segmentation using Instance Boundary Error Estimation and Refinement (INSTA-BEER) across various domains. From the initial segmentation, INSTA-BEER first predicts pixel-wise quad-metric boundary errors. Based on these error estimates, it then performs error-informed segmentation refinement.

[1]–[5] typically train category-agnostic instance segmentation networks on large-scale synthetic datasets to handle diverse objects and environments, serving as the basis for perception modules in various robotic manipulation tasks such as pushing [6], [7], grasping [5], [8], [9], and re-arrangement [10], [11].

The performance of UOIS directly impacts the success of subsequent tasks, necessitating reliable and fast segmentation. Despite advancements in UOIS, existing methods still face challenges in accurately distinguishing object instances in cluttered scenes, with the major problems being over-segmentation and under-segmentation. Over-segmentation is the phenomenon in which a single object is split into multiple segments. It can lead to dropped or damaged objects during grasping. Conversely, under-segmentation is the phenomenon in which distinct objects are merged into a single segment, and it can result in the unintentional grasping of multiple objects simultaneously. Moreover, both errors can lead to object identification failure, making robots grasp the wrong objects. To improve the segmentation quality, fine-grained refinement methods [12]–[15] have been proposed to enhance boundary quality and sharpness by training networks that take coarse initial segmentation masks and predict fine-grained refined masks. However, these methods focus on improving minor fine-grained details and assume that the initial segmentation masks are accurate at an instance level, hindering effective correction of over- and under-segmentation. To mitigate these problems, a recent refinement method [16] was proposed to

provide instance-level refinement by adding new instances or splitting incorrect instances. However, its high computational load limits its practical application in robotics.

In this article, we propose **INSTA** **B**oundary **E**rror **E**stimation and **R**efinement (INSTA-BEER), a novel error-informed refinement method that addresses both fine-grained and instance-level errors in UOIS models for robust unknown object segmentation and grasping. INSTA-BEER first predicts the quad-metric boundary error, which is a pixel-wise representation of true positive (TP), true negative (TN), false positive (FP), and false negative (FN) errors in the instance boundaries of the initial segmentation. By providing specific refinement guidance (e.g., FP to be deleted, FN to be added), the quad-metric boundary error facilitates the subsequent refinement process. Using the Error Guidance Fusion (EGF) module, INSTA-BEER then refines the segmentation with explicit guidance from the estimated errors. As the proposed quad-metric boundary error can effectively represent fine-grained and instance-level segmentation errors and directly informs the refinement process, our method can effectively resolve over- and under-segmentation problems (Fig. 1). We demonstrate that INSTA-BEER consistently improves upon various initial segmentation methods with a fast inference time ( $\sim 0.1$ s @ RTX3090, Intel6248R) by achieving state-of-the-art performance on three widely used benchmarks. Moreover, we demonstrate a practical, real-world robotic application of INSTA-BEER by improving the success rate of target object grasping. The main contributions of this study are summarized as follows:

- We introduce INSTA-BEER, a novel error-informed refinement method that effectively addresses under- and over-segmentation problems in UOIS models, significantly improving segmentation quality with a fast inference time ( $\sim 0.1$ s).
- We propose a quad-metric boundary error estimation to quantify pixel-wise errors at object instance boundaries, capturing both fine-grained and instance-level errors and providing refinement guidance.
- We develop the Error Guidance Fusion (EGF) module, which explicitly integrates the estimated quad-metric boundary errors into the refinement process, guiding the model to produce accurate segmentation improvements.
- We demonstrate the performance and practical applicability of INSTA-BEER through extensive evaluations on benchmark datasets and in real-world robotic grasping.

## II. RELATED WORK

### A. Unknown Object Instance Segmentation

Unknown object instance segmentation (UOIS) [1]–[3] aims to detect all arbitrary object instances in an image where objects and environments are unknown in the test phase. It has been widely used as a fundamental perception module for various robotic manipulation tasks, including object pushing [6], [7], grasping [5], [8], [9], and re-arrangement [10], [11]. Early methods primarily utilized clustering techniques, such as graph-based segmentation [17], surface patches with support vector machines [18], and ambiguity graphs [19]. Recent

state-of-the-art methods employ deep segmentation networks trained on large-scale synthetic data to learn category-agnostic instance segmentation [1]–[5], [20]. These networks learn objectness by distinguishing foreground object instances from the background in RGB-D images, enabling the segmentation of unknown objects in scenarios such as tabletop scenes [18], [21]. However, accurately segmenting objects in cluttered environments remains challenging, particularly when objects overlap, leading to over-segmentation and under-segmentation problems [2], [4], [5], [20], [22]. The proposed method addresses this challenge by refining the initial segmentation from existing UOIS methods to improve segmentation quality in handling cluttered scenes and overlapping objects.

### B. Refining Segmentation

Accurate object segmentation is crucial and directly impacts the performance of subsequent robotic manipulation tasks such as object grasping [8], [9]. To obtain fine-grained segmentation, conditional random fields [23], [24] have been proposed, but they can not handle semantic information and large error regions. Recently, several refinement networks have been proposed to produce fine-grained segmentation. Segfix [13] first detects boundaries, then replaces the predictions of unreliable boundary pixels with the corresponding internal pixel predictions. However, directly predicting accurate instance boundaries is very challenging. Boundary patch refinement (BPR) [15] crops a set of small patches from the boundary of coarse masks and then predicts boundary-aligned patches. CascadePSP [14] takes a coarse initial segmentation mask and predicts more boundary-precise masks in a cascade and coarse-to-fine manner. Although these networks effectively produce fine-grained segmentation, they refine only minor details without correcting errors at the instance level, making it hard to resolve over- and under-segmentation.

To address this limitation, RICE [16] introduced an instance-level refinement method for UOIS by first sampling from instance-level perturbations (adding, deleting, splitting, or merging instances) and selecting the best-scored segmentation using a graph neural network. This allows for the potential refinement of instance-level errors, such as false positives or missing instances. Despite its state-of-the-art performance, RICE depends on multiple sampling operations to find segmentation candidates, leading to a long inference time of up to 10-15 seconds per frame, which hinders its practical application in robotics. Zhang et al. [25] propose a test-time adaptation method to adapt UOIS models to unknown test domains by minimizing entropy; however, this requires approximately 20 seconds for new scenarios. In contrast, our approach enables fast instance-level refinement of less than 0.1 seconds per frame with state-of-the-art performance.

### C. Error Detection for Segmentation and Refinement

Estimating errors in deep segmentation models is essential for ensuring safe and reliable systems [26]. Various methods have been proposed for error detection in segmentation models. Maximum softmax probability [27] and Monte Carlo dropout [28] are common methods for detecting errors in deep

networks by monitoring the probability of network outputs, but they often fall short when applied to segmentation [29], [30]. To address their shortcomings, several approaches have been proposed, including anomaly segmentation methods utilizing uncertainty and re-synthesis [31] and energy-biased abstention learning [32]. Furthermore, integrating a failure detection network with the main segmentation network has been explored to identify pixel-wise failures [30], [33].

Rather than solely focusing on error detection, estimated errors can be leveraged to refine segmentation. Several methods have been proposed for predicting binary mask errors (true and false) in segmentation. Xie et al. [34] proposed using separate networks for segmentation, evaluation, refinement, and verification to achieve accurate semantic segmentation. However, this approach requires separate training steps for each network, increasing the computational complexity. Kuhn et al. [35] introduced an error-reversing autoencoder to correct initial segmentation errors, but it is limited to semantic segmentation and does not address instance grouping. Wang et al. [36] presented a network for refining initial segmentations using an uncertainty map, while Ali et al. [37] developed specific modules for failure detection and label correction. However, these networks require separate trainings from the main segmentation model, adding to the computational cost. In contrast, our proposed method uses only a single network for both error estimation and refinement, eliminating the need for separate training steps and reducing computational complexity. Moreover, we introduce the concept of detecting quad-metric errors (TP, TN, FP, and FN) in instance boundaries, effectively capturing instance-level errors.

### III. PROBLEM STATEMENT

1) *Problem Formulation*: We address the problem of UOIS by refining the quality of initial segmentation models. We formalize the problem using the following definitions:

1. **UOIS**: The objective of UOIS is to identify the set of all object instance masks  $M$  in an RGB-D image  $I$ , where unknown objects are given in the test phase. An object is categorized as unknown if it is not in the training dataset.
2. **Initial segmentation model** ( $\mathcal{F}_{in}$ ): This model, denoted as  $\mathcal{F}_{in} : I \rightarrow M_{in}$ , is any UOIS model that maps the input image  $I$  to a set of initial segmentation masks,  $M_{in}$ .
3. **Segmentation refinement model** ( $\mathcal{F}_{re}$ ): This model, represented by  $\mathcal{F}_{re} : (I, M_{in}) \rightarrow M_{re}$ , aims to improve the quality of initial segmentation masks. It takes the RGB-D image  $I$  and the initial segmentation masks  $M_{in}$  and produces a set of refined segmentation masks  $M_{re}$ .

For a segmentation refinement model, we propose a novel error-informed refinement method comprising the following:

1. **Segmentation errors** ( $e_{in}$ ): These represent the discrepancies between initial segmentation masks  $M_{in}$  and their ground-truth masks. This can be a choice, such as inaccurately classified masks or boundaries.
2. **Error estimator** ( $\mathcal{E}$ ): Denoted as  $\mathcal{E} : (I, M_{in}) \rightarrow e_{in} \sim \hat{e}_{in}$ , this module predicts the segmentation error estimates  $\hat{e}_{in}$ , in the initial segmentation  $M_{in}$ .

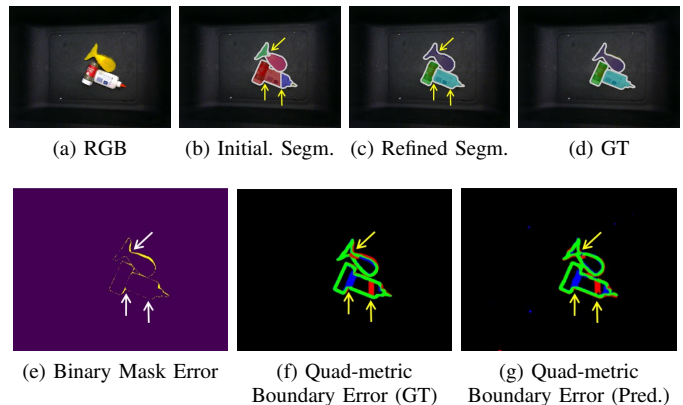


Fig. 2. Comparison of binary mask errors (True, False, shown in (e)) and our quad-metric boundary errors (TP, TN, FP, FN, shown in (f) and (g)) to represent segmentation errors in the initial segmentation (b). The proposed quad-metric boundary errors effectively depict instance-level errors (indicated by arrows) and facilitate precise refined segmentation (c).

3. **Error-informed refiner** ( $\mathcal{H}$ ): This module, denoted as  $\mathcal{H} : (I, M_{in}, \hat{e}_{in}) \rightarrow M_{re}$ , refines the initial segmentation  $M_{in}$  of image  $I$  based on the error estimates  $\hat{e}_{in}$ . Guided by error estimates, this module can focus on the erroneous regions, enabling more accurate and targeted refinement.

Following the proposed error-informed refinement, INSTA-BEER serves as a segmentation refinement model  $\mathcal{F}_{re}$  that aims to enhance the initial segmentations from various UOIS methods. It first predicts error estimates and then refines the segmentation based on these estimates, formulated as follows:

$$\begin{aligned} \mathcal{F}_{re}(I, M_{in}) &= \mathcal{H}(I, M_{in}, \mathcal{E}(I, M_{in})) \\ &= \mathcal{H}(F_{enc}(I, M_{in}), \mathcal{E}(F_{enc}(I, M_{in}))) = M_{re} \end{aligned} \quad (1)$$

In this equation,  $\mathcal{F}_{re}(I, \mathcal{F}_{in})$  denotes the INSTA-BEER model,  $\mathcal{H}(I, M_{in}, \mathcal{E}(I, M_{in}))$  describes the process of error estimation and refinement, and  $M_{re}$  is the refined segmentation result. The function  $F_{enc}(I, M_{in})$  indicates the encoded features of  $I$  and  $M_{in}$  derived from the feature extractor  $F_{enc}$ . Leveraging this error-informed refinement scheme enables INSTA-BEER to explicitly predict and incorporate the segmentation errors for a structured and precise refinement process. In particular, we introduce quad-metric boundary errors as the segmentation errors  $e_{in}$  (Subsection III-2) and propose an error guidance fusion (EGF) module to seamlessly incorporate these estimated errors into the refinement process (Section IV).

2) *Quad-metric Boundary Error*: To effectively capture instance-level errors and provide explicit refinement guidance, we introduce quad-metric boundary errors as the segmentation error  $e_{in}$ . Fig. 2 compares the binary mask errors and our proposed quad-metric boundary errors.

**Binary mask errors** (Fig. 2e), a typical representation used in error detection methods [34], [35], are pixel-wise binary discrepancy (true or false) between segmentation masks and ground truths, expressed as  $\{0, 1\}^{w \times h}$ , where  $w$  and  $h$  are image width and height. While binary mask errors can represent minor misalignment between IS and ground truth, identifying instance-level errors in overlapping instances, such as under-segmentation and over-segmentation, is challenging.

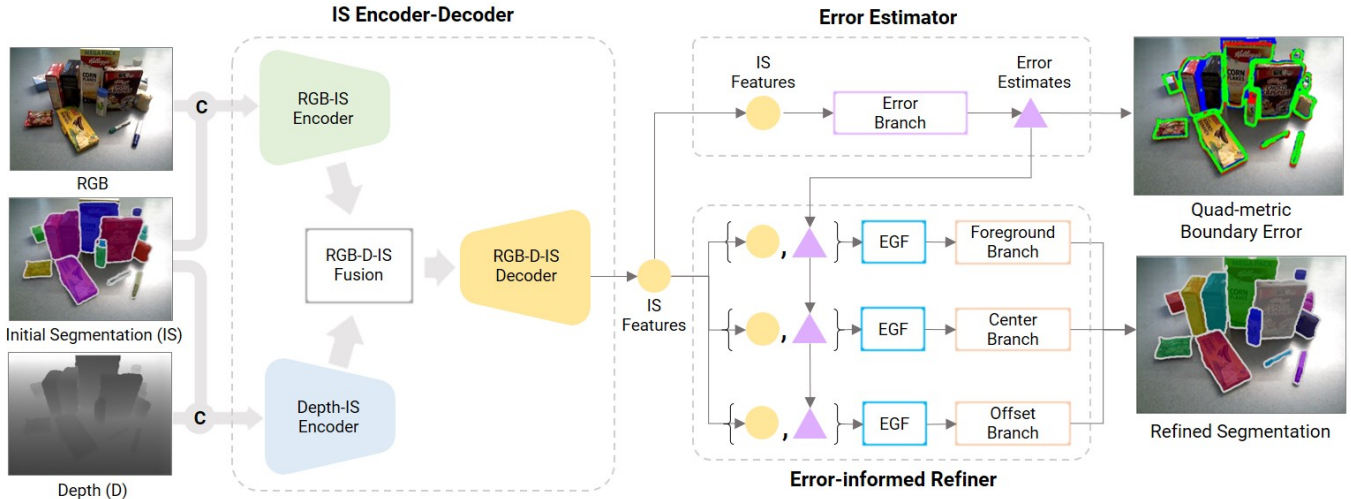


Fig. 3. Overview of the INSTA-BEER for error-informed refinement. The initial segmentation (IS) feature extractor generates IS features from RGB-D and IS inputs. Then, the error estimator predicts quad-metric boundary errors in the initial segmentation. The EGF module integrates these estimated errors into the refinement process. The error-informed refiner produces the refined segmentation, representing instances as a set of foreground, center, and offset.

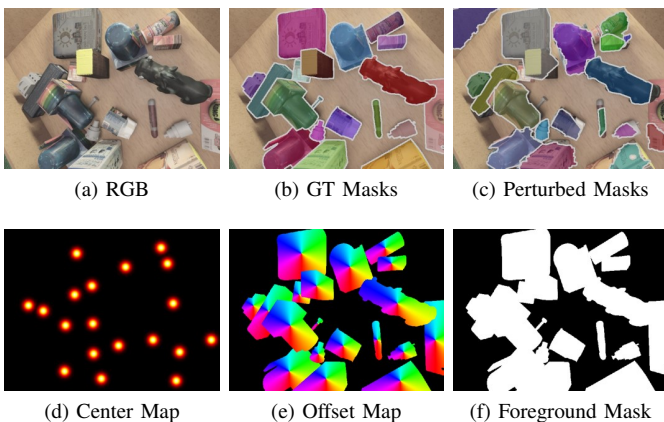


Fig. 4. Example of RGB, GT masks, and corresponding perturbed masks used in training (first row) on UOAI-SIM dataset, and center map, offset map, and foreground mask for instance representation (second row).

Moreover, binary mask errors only indicate whether specific pixels are correctly or wrongly classified, leading to ambiguity in the refinement process, as they do not clearly distinguish the error types, whether false pixels are inaccurately segmented pixels (FP) and missing object pixels (FN).

To address these limitations, **quad-metric boundary errors** (Fig. 2f) are utilized as a segmentation error in the error estimator, which are pixel-wise TP, TN, FP, and FN errors on instance boundaries. It is computed by first obtaining the boundaries of all IS and GT instance masks using a dilation operation [38]. Then, instance boundary maps for IS and GT are constructed by taking the union of the dilated boundaries. Finally, the pixel-wise TP, TN, FP, and FN errors are evaluated between the instance boundary maps of IS and GT, resulting in  $\{0, 1\}^{w \times h \times 4}$ . By focusing on the instance boundaries, these errors provide a more precise and localized representation of instance-level errors in overlapping instances. Furthermore, quad-metric boundary errors provide explicit guidance for the

refinement process, indicating that the pixels are accurately segmented (TP, TN), inaccurately segmented (FP), or missing object pixels (FN). By predicting this error (Fig. 2g), our model could produce accurate refined segmentation (Fig. 2c) by resolving the over- and under-segmentation.

#### IV. INSTA-BEER

The INSTA-BEER employs an error-informed refinement scheme that decomposes the refinement process into error estimation and error-informed refinement steps. It consists of three main components (Fig. 3): 1) initial segmentation feature extractor  $F_{enc}$ , which extracts initial segmentation (IS) features from the input RGB-D image and IS masks; 2) error estimator  $\mathcal{E}$ , which predicts pixel-wise quad-metric boundary errors in the IS; and 3) error-informed refiner  $\mathcal{H}$ , which refines the IS with guidance of the estimated errors. The error guidance fusion (EGF) modules leverage both IS features and error estimates for targeted and effective refinement.

##### A. Initial Segmentation Feature Extractor

The IS feature extractor takes RGB, depth (D), and IS as inputs and extracts the IS features, which are used for subsequent error estimation and refinement. We employ two parallel ResNet-50 backbones [39], termed RGB-IS and Depth-IS encoders to extract modality-specific features conditioned on IS. These take the input of concatenation of IS with RGB and depth, respectively. As an IS representation, we utilize a center map, an offset map, and a foreground mask, which are described in Subsection IV-E. Then, the RGB-D-IS fusion process combines the features obtained from the RGB-IS and Depth-IS encoders at specific stages: after the second, third, and fifth residual blocks (C2, C3, and C5, respectively). First, the RGB-IS and Depth-IS features are concatenated. Then, the fused features are processed using a series of convolutions: one  $1 \times 1$  and two  $3 \times 3$  convolutions. At the C5 stage, only  $1 \times 1$

convolutions are used to maintain computational efficiency while still capturing high-level semantic information.

Following this, the features at the C5 stage are processed through an atrous spatial pyramid pooling (ASPP) [24] module to extract multi-scale contextual information, similar to Panoptic-DeepLab [40]. Finally, the decoder generates IS features ( $c \times p \times q$ ) by upscaling the resolution using  $5 \times 5$  depthwise-separable convolutions while reintegrating features from the C2 and C3 stages through  $1 \times 1$  convolutions. This multi-scale feature fusion approach enhances the spatial resolution and captures fine-grained details essential for accurate segmentation refinement. The  $c$ ,  $p$ , and  $q$  represent the number of channels, feature width, and feature height, respectively.

### B. Error Estimator and Error-informed Refiner

The error estimator  $\mathcal{E}$  predicts the quad-metric boundary error in the initial segmentation (IS) to guide the refinement process. It takes IS features as input and generates error features using  $5 \times 5$  depthwise separable convolutions [41], which are then processed through  $1 \times 1$  convolutions to produce quad-metric boundary error maps ( $4 \times p \times q$ ).

The error-informed refiner  $\mathcal{H}$  consists of separate branches for predicting foreground, center, and offset maps. Each branch incorporates its own error guidance fusion (EGF) module, a key component responsible for integrating the predicted error estimates (error features and error maps) with the IS features. The EGF modules take the error maps, error features, and IS features as inputs and combine them using a  $1 \times 1$  convolution to reduce the number of channels from  $2c + 4$  to  $c$ , followed by feature extraction using three  $3 \times 3$  convolutions.

By fusing both error features and error maps, the refiner can adapt its predictions based on the error information, thereby enhancing the accuracy of the final output. Notably, the quad-metric boundary error is used as a segmentation error instead of a binary mask error, enabling the EGF module to encode crucial information on which pixels contain errors and provide valuable insights into how to refine them. This fine-grained error information enables the refiner to make more targeted and effective adjustments to the initial segmentation.

The error-informed refiner branches predict the foreground, center, and offset maps using  $5 \times 5$  depthwise separable and  $1 \times 1$  convolutions, drawing inspiration from the approach in [40]. Non-maximum suppression and a hard threshold are then applied to the center maps to eliminate low-confidence centers. Finally, the foreground pixels are grouped with their nearest center using the center and offset maps to form the final, refined instance masks.

### C. Comparison with Panoptic-DeepLab

Our proposed model builds upon the fast end-to-end single-shot network Panoptic-DeepLab [40], which also utilizes the ASPP module for multi-scale feature extraction and predicts foreground, center, and offset maps. However, our model introduces several novel ideas for category-agnostic refinement from RGB-D and IS, setting it apart from Panoptic-DeepLab. First, while Panoptic-DeepLab generates IS from

RGB images, our model is specifically designed for the error-informed refinement of IS, introducing an error estimator and EGF modules to facilitate this process. Second, our model employs RGB-IS and Depth-IS encoders to fuse RGB, depth, and IS information effectively, enabling it to capture more comprehensive and accurate scene representations. Finally, we utilize a class-agnostic foreground branch instead of a separate semantic segmentation branch to reduce computational costs and make our model more efficient and suitable for real-time applications. These enable our model to achieve state-of-the-art performance in category-agnostic instance segmentation refinement from RGB-D and IS, and ablation studies are presented in Section V-D1.

### D. Mask perturbation

To refine the initial segmentation (IS) from arbitrary UOIS models, we generate perturbed masks (Fig. 4c) by applying random perturbations to the ground truth masks and use them as IS during training. An alternative approach is to use the predictions of UOIS models for training. However, training on a specific set of UOIS model predictions can reduce adaptability to untrained UOIS models. Moreover, UOIS models are typically trained on large-scale synthetic images, and these models often produce accurate segmentations on synthetic training sets, which cover only a small distribution of segmentation error types. In contrast, our mask perturbation method introduces a wider distribution of potential segmentation errors, enabling a more robust refinement.

We simulate both fine-grained and instance-level segmentation errors by combining mask perturbation methods from existing approaches [14], [16] to cover various types of segmentation errors produced by UOIS models. To mimic fine-grained errors, we apply contour subsampling, random dilation, and erosion from [14]. For instance-level errors, we use random mask removal and splitting of neighboring masks, as described in [16]. Additionally, we introduce random false positive instances using graph segmentation [17]. Fig. 4c shows an example of perturbed masks used in training, which include both fine-grained (minor misalignment on boundaries) and instance-level segmentation errors (missing instances, wrongly detected instances, merged or split instances).

### E. Instance Representation Details

We use a set of the center map, offset map, and foreground (Fig. 4d, 4e, 4f) for both IS inputs and prediction targets in our network. The center map ( $w \times h \times 1$ ) represents the probability of each pixel being an instance center, while the offset map ( $w \times h \times 2$ ) represents the x and y offsets from each pixel to its closest instance center. The foreground is the binary map indicating whether each pixel is the foreground (object) or not ( $w \times h \times 1$ ). This representation was originally used in [40] for predicting instances, but we also use it as an IS input, as it ensures a fixed-shape representation of the IS, regardless of the total number of instances in the IS, allowing for the encoders to capture both the spatial and relational information of the initial segmentation. For the IS input, we concatenate the center map and offset maps ( $IS \in \mathcal{R}^{w \times h \times 3}$ )

## F. Implementation Details

During the training of the INSTA-BEER model, we used several loss functions: dice loss for error estimation ( $L_{err}$ ), cross-entropy loss for foreground segmentation ( $L_{fg}$ ), MSE loss for center map ( $L_{ctr}$ ) [42], and L1 loss for offset map ( $L_{off}$ ) [43]. The total loss  $L$  is computed as follows:

$$L = \lambda_{err}L_{err} + \lambda_{fg}L_{fg} + \lambda_{ctr}L_{ctr} + \lambda_{off}L_{off} \quad (2)$$

To balance the contributions of each loss term, we set  $\lambda_{err} = 1$ ,  $\lambda_{fg} = 1$ ,  $\lambda_{ctr} = 200$ , and  $\lambda_{off} = 0.01$ . INSTA-BEER, including the error estimator and error-informed refinements, is jointly trained in an end-to-end manner.

Our models are trained on synthetic datasets and evaluated on real images without any fine-tuning, following the standard protocol in UOIS methods [3]–[5], [16]. For training, we employed two datasets: UOAI-SIM (Fig. 4) [5] and TOD [3], [16], which comprise 50k photorealistic and 100k non-photorealistic synthetic images, respectively. We trained separate models on each dataset to ensure a fair comparison with other methods. The model was trained for 90k iterations using the Adam optimizer [44], with a learning rate of 0.000125 and batch size of 8. We also used color [45] and depth augmentation [46] for the sim-to-real transfer. The image size was  $640 \times 480$  for both training and testing. The training process took approximately 21 hours on two RTX 3090 GPUs.

In line with the approach proposed in [5], a lightweight foreground segmentation [47] model trained on the TOD dataset [2] was used to filter out background instances, using an overlap ratio of 0.3. As in [2], [3], noisy masks smaller than 500 pixels were removed. We used the ResNet-50 backbone pre-trained on ImageNet [48], and 0.3 for center threshold during post-processing.

## V. EXPERIMENTS

### A. Datasets and Metrics

We evaluated the models on three widely used benchmark datasets of real-world cluttered scenes: OCID [21], OSD [18], and WISDOM [1]. The OCID dataset consists of 2,346 indoor images, including both tabletop and floor scenes, with semi-automated labels. It features an average of 7.5 objects per image, with a maximum of 20 objects. The OSD dataset contains 111 images of tabletop scenes with human-annotated ground truths, having an average of 3.3 objects per image and a maximum of 15 objects. The WISDOM dataset comprises 300 test images of bin scenes with human-annotated ground truths, an average of 3.8 objects per image, and a maximum of 11 objects. Importantly, the test objects in these datasets do not overlap with those in the training set, allowing for the performance evaluation on unknown objects.

To compare the segmentation performance, we employed standard metrics [16]: object size normalized (OSN) overlap precision, recall, and F-measure ( $P_n^O, R_n^O, F_n^O$ ), as well as OSN boundary precision, recall, and F-measure ( $P_n^B, R_n^B, F_n^B$ ). These metrics are used to evaluate the segmentation performance over masks and boundaries, fairly considering both large and small objects, independent of their sizes. Given the Hungarian assignment  $A$  between the

$N$  predicted and  $M$  ground truth instance masks, the OSN overlap measures were computed as follows:

$$P_n^O = \frac{\sum_{(i,j) \in A} P_{ij}}{N}, R_n^O = \frac{\sum_{(i,j) \in A} R_{ij}}{M}, F_n^O = \frac{\sum_{(i,j) \in A} F_{ij}}{\max(M, N)} \quad (3)$$

where  $P_{ij}$ ,  $R_{ij}$ , and  $F_{ij}$  represent the precision, recall, and F-measure between predicted and ground truth instance masks, respectively. Similarly, the OSN boundary precision, recall, and F-measure are computed using the boundary pixels obtained through a dilation operation. Additionally, we used the percentage of segmented objects with OSN overlap  $F_n^O \geq 0.75$  (@.75) to measure the proportion of objects segmented with a high accuracy [49]. The reported metrics for INSTA-BEER are the averages of three measurements.

Considering the importance of computational efficiency in robotic applications, we also evaluated the inference time required to process a single frame. Using UCN [4] as the IS model, we measured the average and standard deviation of times for refining the segmentation for each dataset, including post-processing. For a fair comparison, we used the same hardware for this measurement on a single RTX 3090 GPU and an Intel Xeon Gold 6248R processor. It is worth noting that computational costs can vary based on dataset characteristics and the number of instances. For example, CascadePSP refines the segmentation per instance, and the sample operation of the RICE method grows with the number of instances. Similarly, the inference time of INSTA-BEER can vary due to post-processing in merging instances.

### B. Comparison with State-of-the-Art Methods

1) *Experiment Setup*: We compared our INSTA-BEER with three refinement models: BPR [15], CascadePSP [14], and RICE [16]. BPR is a fine-grained segmentation refinement model that first crops small patches from the boundary of the IS and then refines them using an HRNet-48 [50] encoder-decoder network. CascadePSP [14] is another fine-grained segmentation refinement model that takes an individual instance mask as input and refines it using PSPNet [51] in a coarse-to-fine manner. RICE [16] is an instance-level refinement network that first samples instance-level perturbations, including splitting, merging, adding, and deleting, and then selects the best-scored segmentation using a graph neural network.

For BPR and CascadePSP, we trained the models on UOAI-SIM [5] using their official codes. We modified the input channels of both models to take RGB-D image inputs (concatenation of RGB and depth channels) for a fair comparison with RGB-D methods; RICE and INSTA-BEER. For RICE, we used the official pre-trained weights trained on the TOD dataset [3], [16]. INSTA-BEER was trained on two different datasets: one version was trained on UOAI-SIM and subsequently compared with BPR and CascadePSP; the other was trained on TOD [3], [16] and compared with RICE.

To evaluate the adaptability of the refinement methods to various IS, we used five state-of-the-art UOIS methods as IS models: Detic [52], UOIS-Net-3D [3], UOAI-Net [5], MSMFormer [20], and UCN [4] (the last two models include zoom refinement), using their official codes. For Detic, a

TABLE I

PERFORMANCE COMPARISON OF INSTA-BEER WITH THE FINE-GRAINED SEGMENTATION REFINEMENT MODELS, BPR AND CASCADEPSP, ON THE OSD AND OCID ACROSS FIVE INITIAL SEGMENTATION MODELS. ALL REFINEMENT MODELS WERE TRAINED ON THE UOAI-SIM DATASET.

dataset	refinement methods	inference time (s)	Detic			UOIS-Net-3D			UOAI-Sim			MSMFormer			UCN			Average
			$F_n^O$	$F_n^B$	@.75													
OCID	without refinement	-	68.3	67.6	71.2	77.4	74.2	76.3	66.7	64.4	66.5	81.9	81.3	81.6	84.1	83.0	84.9	75.3
	+ BPR	0.094±0.031	67.4	63.7	70.1	76.9	70.9	75.6	65.2	61.5	64.8	80.1	74.2	80.8	83.2	77.5	84.5	73.1 (-2.2)
	+ CascadePSP	2.099±1.501	68.7	66.8	71.3	78.6	76.9	77.2	67.0	65.8	66.4	81.8	81.3	81.8	84.1	83.6	84.9	75.9 (+0.6)
	+ INSTA-BEER	<b>0.091±0.017</b>	<b>79.4</b>	<b>77.5</b>	<b>80.7</b>	<b>84.2</b>	<b>81.5</b>	<b>84.6</b>	<b>78.6</b>	<b>75.7</b>	<b>78.0</b>	<b>85.6</b>	<b>83.2</b>	<b>86.7</b>	<b>86.1</b>	<b>83.7</b>	<b>87.6</b>	<b>82.2 (+6.9)</b>
OSD	without refinement	-	63.1	61.0	62.5	75.0	69.8	70.4	75.7	68.6	71.5	77.0	63.4	75.7	77.0	65.0	76.2	70.0
	+ BPR	0.087±0.028	61.8	55.5	62.5	73.8	66.9	69.2	74.7	67.6	71.3	77.6	69.3	75.9	78.7	69.9	77.1	70.1 (+0.1)
	+ CascadePSP	1.370±1.479	62.8	57.9	63.0	74.7	67.9	70.0	75.9	68.2	71.4	78.3	67.8	76.5	78.3	68.3	76.8	70.5 (+0.5)
	+ INSTA-BEER	<b>0.083±0.015</b>	<b>70.2</b>	<b>64.1</b>	<b>66.8</b>	<b>80.5</b>	<b>73.5</b>	<b>77.1</b>	<b>81.8</b>	<b>74.7</b>	<b>79.0</b>	<b>81.0</b>	<b>73.2</b>	<b>78.4</b>	<b>82.9</b>	<b>75.3</b>	<b>80.8</b>	<b>76.0 (+6.0)</b>

TABLE II

PERFORMANCE COMPARISON OF INSTA-BEER WITH THE INSTANCE-LEVEL REFINEMENT MODEL, RICE, ON THE OSD AND OCID ACROSS FIVE INITIAL SEGMENTATION MODELS. ALL REFINEMENT MODELS WERE TRAINED ON THE TOD DATASET.

dataset	refinement methods	inference time (s)	Detic			UOIS-Net-3D			UOAI-Sim			MSMFormer			UCN			Average
			$F_n^O$	$F_n^B$	@.75													
OCID	without refinement	-	68.3	67.6	71.2	77.4	74.2	76.3	66.7	64.4	66.5	81.9	81.3	81.6	84.1	83.0	84.9	75.3
	+ RICE-fast	0.654±0.199	73.7	72.8	76.3	79.7	76.3	79.5	67.8	65.3	67.8	83.0	82.0	83.2	85.1	83.9	86.2	77.5 (+2.2)
	+ RICE-default	2.349±1.610	77.3	75.8	80.0	<b>82.9</b>	<b>79.1</b>	<b>84.3</b>	69.4	66.6	70.0	<b>84.8</b>	<b>83.4</b>	<b>85.7</b>	<b>86.4</b>	<b>84.8</b>	<b>87.8</b>	79.9 (+4.6)
	+ INSTA-BEER	<b>0.091±0.017</b>	<b>84.4</b>	<b>81.4</b>	<b>85.7</b>	80.0	77.5	79.5	<b>79.8</b>	<b>76.4</b>	<b>79.3</b>	82.8	80.3	83.4	85.5	83.0	87.0	<b>81.7 (+6.4)</b>
OSD	without refinement	-	63.1	61.0	62.5	75.0	69.8	70.4	75.7	68.6	71.5	77.0	63.4	75.7	77.0	65.0	76.2	70.0
	+ RICE-fast	0.631±0.304	67.2	63.8	65.6	77.4	71.1	74.8	75.5	68.0	71.4	79.4	64.7	78.8	78.9	66.3	79.5	72.2 (+2.2)
	+ RICE-default	2.342±2.015	71.2	66.3	70.5	<b>78.4</b>	<b>71.4</b>	<b>76.1</b>	77.6	69.6	74.5	<b>79.3</b>	64.3	<b>79.2</b>	<b>79.9</b>	66.9	<b>80.0</b>	73.7 (+3.7)
	+ INSTA-BEER	<b>0.083±0.015</b>	<b>79.4</b>	<b>71.3</b>	<b>77.3</b>	76.1	68.6	71.5	<b>80.5</b>	<b>72.5</b>	<b>76.3</b>	77.3	<b>68.5</b>	74.6	<b>79.9</b>	<b>71.6</b>	77.2	<b>74.8 (+4.8)</b>

TABLE III

PERFORMANCE COMPARISON ON THE WISDOM DATASET. MODELS WITH † WERE TRAINED ON TOD; OTHERS WERE TRAINED ON UOAI-SIM.

refinement methods	UOAI-Sim			MSMFormer			UCN			Average
	$F_n^O$	$F_n^B$	@.75	$F_n^O$	$F_n^B$	@.75	$F_n^O$	$F_n^B$	@.75	
without refinement	72.8	65.7	73.3	75.3	67.5	76.8	67.8	60.0	68.0	69.7
BPR	78.4	71.0	79.8	77.0	69.4	78.9	69.9	63.2	69.8	73.0 (+3.3)
CascadePSP	78.4	71.3	79.0	77.4	70.2	78.7	68.9	61.9	68.8	72.7 (+3.0)
<b>INSTA-BEER</b>	<b>78.5</b>	<b>70.9</b>	<b>80.8</b>	<b>79.7</b>	<b>71.7</b>	<b>81.9</b>	<b>74.8</b>	<b>67.3</b>	<b>75.8</b>	<b>75.7 (+5.0)</b>
RICE-fast †	77.0	69.6	77.9	76.7	68.4	78.2	72.0	63.3	72.5	72.8 (+3.1)
RICE-default †	78.4	70.7	79.5	<b>78.1</b>	69.2	<b>80.2</b>	<b>75.4</b>	66.0	<b>75.9</b>	74.8 (+5.1)
<b>INSTA-BEER †</b>	<b>81.0</b>	<b>73.1</b>	<b>82.2</b>	77.8	<b>69.7</b>	79.2	74.1	<b>66.3</b>	74.3	<b>75.3 (+5.6)</b>

universal open vocabulary IS model to segment objects from a given vocabulary, we used class names (e.g., banana, keyboard, cereal box) as custom vocabulary. Note that all initial segmentation and refinement methods take RGB-D images as input, except for Detic, which only uses RGB images.

### 2) Comparison with Fine-grained Refinement Models:

Table I compares the performance of INSTA-BEER with BPR [15] and CascadePSP [14], which are state-of-the-art fine-grained segmentation refinement models, on the OCID and OSD datasets. INSTA-BEER achieves superior segmentation performance compared to BPR and CascadePSP, improving the average performance across five IS models from 75.3 to 82.2 (+6.9) on OCID and 70.0 to 76.0 (+6.0) on OSD. Moreover, it achieves the fastest inference time, which is less than 0.1 seconds. In contrast, BPR and CascadePSP lead to

only minor improvements over the initial segmentation (IS), with BPR even worsening the segmentation performance on OCID. This can be attributed to their primary focus on fine-grained segmentation details without instance-level refinement capabilities, leading to failures in handling over- and under-segmentation issues.

3) Comparison with Instance-level Refinement Model: We also compare the performance of INSTA-BEER with RICE [16], the instance-level refinement method, on the OCID and OSD datasets in Table II. We report two versions of RICE; RICE-default uses the default number of instance-level sampling operations as reported in the paper ( $B = 3$ ,  $N = 1$ ,  $K = 1750$ ), while RICE-fast uses a reduced number of sampling operations ( $B = 1$ ,  $N = 1$ ,  $K = 300$ ) for a fast inference time, where  $B$  and  $N$  denote the maximum allowed number of sampling operations for each instance and all instances, respectively, and  $K$  represents the total number of sampling operations. The results show that our INSTA-BEER achieves a better average improvement across five IS models, from 75.3 to 81.7 (+6.4) on OCID, and 70.0 to 74.8 (+4.8) on OSD, than both RICE-fast and RICE-default. Although RICE performs slightly better than INSTA-BEER in some cases, such as on OCID with UCN as the IS model, our model is significantly faster than both RICE-fast and RICE-default, as they heavily depend on instance-level sampling operations that require high computational cost, making INSTA-BEER more suitable for practical robotic applications.

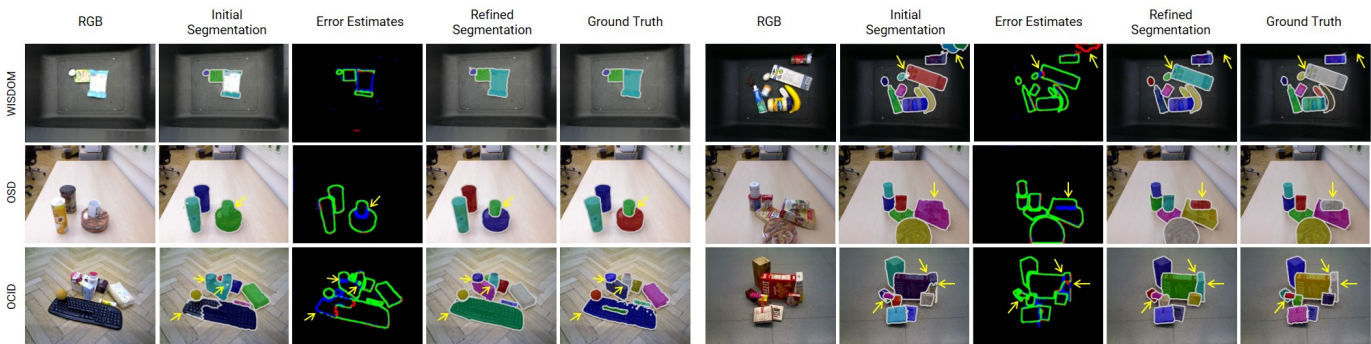


Fig. 5. Visualization of segmentation refinement with INSTA-BEER, correcting over- and under-segmentation in initial UCN segmentation.

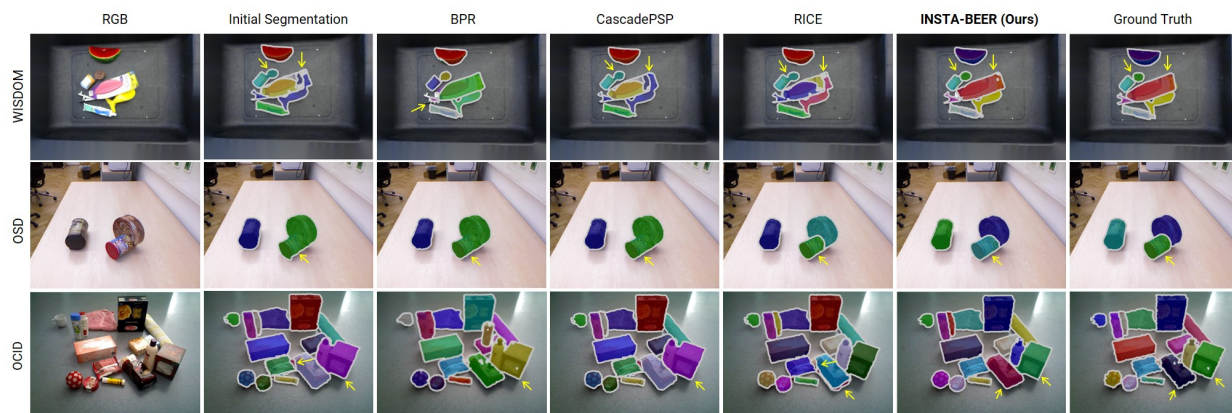


Fig. 6. Qualitative comparison between INSTA-BEER and other refinement models using the same initial segmentation (UCN).

4) *Performance on WISDOM datasets:* We further compare the performance of segmentation refinement methods on the WISDOM dataset in Table III. We report the performance of two versions of INSTA-BEER: one trained on the UOAI-SIM and another trained on the TOD. BPR and CascadePSP were trained on the UOAI-SIM dataset, while RICE was trained on the TOD dataset. The results demonstrate that INSTA-BEER consistently outperforms BPR and CascadePSP. Additionally, our model surpasses RICE-fast on all IS models and achieves similar or better performance than RICE-default, confirming the effectiveness of the proposed method.

### C. Qualitative Results

Fig. 5 shows the effectiveness of INSTA-BEER in refining instance segmentation results on the OSD, OCID, and WISDOM datasets. The visualization demonstrates that INSTA-BEER successfully resolves instance-level segmentation errors in the initial segmentation (UCN) by first estimating the quad-metric boundary errors and then refining the segmentation based on these estimates. Fig. 6 presents a qualitative comparison of INSTA-BEER with other state-of-the-art refinement methods. BPR and CascadePSP refine fine-grained details but fail to correct instance-level errors. RICE tends to correct instance-level errors in some cases but fails to produce accurate instances consistently, as it relies on a sampling strategy that may not cover all scenarios. In contrast, INSTA-BEER successfully refines both fine-grained and instance-level errors.

TABLE IV  
ABLATION EXPERIMENT OF SEGMENTATION REFINEMENT, ERROR ESTIMATION, AND EGF ON OCID. (†: UCN [4] PAPER VALUES)

methods	segm. refine.	error estim.	EGF	$F_n^O$	$F_n^B$	@.75
UCN †	×	×	×	84.2	83.2	85.0
UCN	×	×	×	84.1	83.0	84.9
Panoptic DeepLab	×	×	×	80.4	71.3	76.4
UCN + Panoptic DeepLab	✓	×	×	82.2	77.2	81.0
UCN + INSTA-BEER	✓	✓	×	84.7	81.3	85.3
UCN + INSTA-BEER	✓	✓	✓	<b>86.1</b>	<b>83.7</b>	<b>87.6</b>

TABLE V  
ABLATION EXPERIMENT OF QUAD-METRIC BOUNDARY ERROR ON OCID

quad-metric error	boundary error	overlap			boundary			@.75
		$P_n^O$	$R_n^O$	$F_n^O$	$P_n^O$	$R_n^O$	$F_n^O$	
×	✓	88.2	88.5	84.6	84.0	85.3	81.5	85.4
✓	×	<b>88.9</b>	89.3	85.8	85.7	86.4	83.1	87.3
✓	✓	<b>88.9</b>	<b>89.8</b>	<b>86.1</b>	<b>86.1</b>	<b>87.1</b>	<b>83.7</b>	<b>87.6</b>

TABLE VI  
ABLATION EXPERIMENT OF ERROR FEATURES AND ERROR MAPS IN EGF

error features	error maps	overlap			boundary			@.75
		$P_n^O$	$R_n^O$	$F_n^O$	$P_n^O$	$R_n^O$	$F_n^O$	
×	×	<b>89.0</b>	84.4	82.2	80.1	80.4	77.2	81.0
×	✓	88.8	89.0	85.5	84.8	86.1	82.4	87.0
✓	×	88.7	89.2	85.6	85.5	86.8	83.1	87.1
✓	✓	88.9	<b>89.8</b>	<b>86.1</b>	<b>86.1</b>	<b>87.1</b>	<b>83.7</b>	<b>87.6</b>

TABLE VII

ABLATION EXPERIMENT ON MASK PERTURBATION IN TRAINING (IM: INITIAL SEGMENTATION MODEL MASK, MP: MASK PERTURBATION)

methods	OSD			OCID		
	$F_n^O$	$F_n^B$	@.75	$F_n^O$	$F_n^B$	@.75
IM	81.6	72.6	79.6	81.3	78.4	81.0
IM + MP	82.0	74.2	79.6	82.7	80.0	82.1
MP	<b>82.9</b>	<b>75.3</b>	<b>80.8</b>	<b>86.1</b>	<b>83.7</b>	<b>87.6</b>

TABLE VIII

REAL-WORLD RESULTS ON ROBOTIC TARGET OBJECT GRASPING

methods	segmentation	grasp
	success rate	success rate
UCN	65%	59%
+ INSTA-BEER	<b>82%</b>	<b>75%</b>
UOAIIS-Net	80%	70%
+ INSTA-BEER	<b>86%</b>	<b>76%</b>

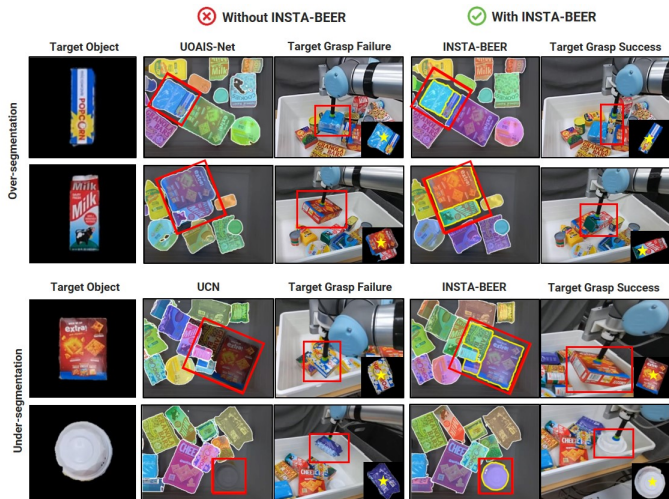


Fig. 7. Real-world robot experiments for target object grasping. INSTA-BEER improves success rates by refining initial UOIS results. Yellow stars indicate grasping points from segmentation. Supplementary videos: <https://sites.google.com/view/insta-beer>.

#### D. Ablation Studies

1) *Effect of Error Estimation and EGF*: We performed ablation studies on error estimation and EGF modules on the OCID dataset, using UCN [4] as the IS model (Table IV). Additionally, we compared INSTA-BEER with the original Panoptic-DeepLab [40]. This model, lacking the error estimator and EGF module, was evaluated as both an IS and a refinement model. For a fair comparison, Panoptic-DeepLab utilized RGB-D inputs, as did INSTA-BEER, and used the IS input when employed as a refinement model. The results demonstrate that Panoptic-DeepLab as an IS model (third row), fails to achieve state-of-the-art performance. Moreover, without error estimation and EGF, Panoptic-DeepLab, as a segmentation refinement model (fourth row) does not improve upon IS and even exhibits a slight decline in performance compared to UCN’s IS (second row). In contrast, the INSTA-BEER model, which employs both error estimation and EGF, significantly surpasses the performance of IS

2) *Effect of Quad-Metric Boundary Error*: To evaluate the importance of the proposed quad-metric boundary error, we performed an ablation study on the OCID dataset using UCN as the IS model (Table V). We compared the performance when predicting 1) the binary mask error at boundaries (first row), 2) the mask quad-metric error (second row), and 3) the quad-metric boundary error at boundaries (third row). The results suggest that the combination of quad-metric error and boundary error yields the best performance, highlighting the

effectiveness of the proposed quad-metric boundary error.

3) *Effect of Error Features and Error Maps in EGF*: We further compared the performance of INSTA-BEER to assess the contribution of error features and error maps in the EGF module on the OCID dataset using UCN (Table VI). The results indicate that incorporating both error features and error maps into the EGF of the error-informed refiner enhances overall performance, suggesting that comprehensive guidance from the error estimator to the error-informed refiner is crucial.

4) *Effect of Mask Perturbation*: Table VII presents the results of the ablation study on mask perturbation methods when training INSTA-BEER on UOAIIS-SIM and testing on OCID. The first row (IM) represents cases where INSTA-BEER is trained on the predictions of IS models [2]–[4], [20]. The third row (MP) represents cases where the mask perturbation described in Section IV-D is used. The second row represents a combination of IS and IM inputs in a 1:1 ratio. The results show that utilizing mask perturbation yields the best performance as our mask perturbation strategy effectively captures a wider range of segmentation errors.

#### E. Robotics Experiment: Target Object Grasping

We evaluated the impact of UOIS refinement using INSTA-BEER on a target object-grasping experiment (Fig. 7). The objective was to detect and grasp a target object from a cluttered bin, where all objects were unknown, and only ten template images were provided per object. The segmentation and grasping pipeline consists of three steps: 1) segmenting the RGB-D images using an IS model with an optional refinement using INSTA-BEER, 2) matching the segmented objects to the templates using the cosine distance of the pre-trained DINOv2 features [53], and 3) executing a suction grasp by identifying the most planar regions using RANSAC plane fitting.

We compared the performance with and without refinement using INSTA-BEER, based on the initial segmentation (IS) from UOAIIS-Net [5] and UCN [4]. We evaluated two metrics: 1) segmentation success rate, defined as whether the target objects were correctly segmented and matched without over- or under-segmentation, and 2) grasp success rate, defined as whether a grasp was successful if the target object was removed from the bin. In each trial, up to 20 objects, including the target and distractors, were randomly placed in the bin. We selected ten target objects and repeated the grasping sequence ten times for each target, resulting in 100 trials to evaluate each method. To ensure consistency, object placements remained the same across trials with and without refinement.

Table VIII presents the segmentation and grasping performance for the target objects. INSTA-BEER leads to im-

improvements in both segmentation and grasp success rates. In particular, INSTA-BEER effectively refines the over-/under-segmentation issues for UOAIS-Net, leading to better matching and grasping. For UCN, which is optimized for tabletop scenarios, INSTA-BEER significantly mitigates its tendency to misdetect target objects in cluttered bin environments by providing enhanced segmentation capabilities.

## VI. CONCLUSION

This study introduces INSTA-BEER, a fast, accurate error-informed refinement method that addresses fine-grained and instance-level errors in UOIS. By predicting the quad-metric boundary error and integrating it into the EGF module, our method achieved state-of-the-art performance on benchmarks. Ablation studies confirmed the effectiveness of the proposed components, and real-world experiments highlighted the impact on target object grasping. The results show that INSTA-BEER promotes UOIS refinement, offering a promising solution for robotic perception in unstructured environments.

## REFERENCES

- [1] M. Danielczuk, M. Matl, S. Gupta, A. Li, A. Lee, J. Mahler, and K. Goldberg, "Segmenting unknown 3d objects from real depth images using mask r-cnn trained on synthetic data," in *Proc. IEEE Int. Conf. Robot. Automat.*, 2019, pp. 7283–7290.
- [2] C. Xie, Y. Xiang, A. Mousavian, and D. Fox, "The best of both modes: Separately leveraging rgb and depth for unseen object instance segmentation," in *Proc. Conf. Robot Learn.*, 2020, pp. 1369–1378.
- [3] —, "Unseen object instance segmentation for robotic environments," *IEEE Trans. Robot.*, 2021.
- [4] Y. Xiang, C. Xie, A. Mousavian, and D. Fox, "Learning rgb-d feature embeddings for unseen object instance segmentation," in *Proc. Conf. Robot Learn.*, 2021, pp. 461–470.
- [5] S. Back, J. Lee, T. Kim, S. Noh, R. Kang, S. Bak, and K. Lee, "Unseen object amodal instance segmentation via hierarchical occlusion modeling," in *Proc. IEEE Int. Conf. Robot. Automat.*, 2022, pp. 5085–5092.
- [6] H. Yu and C. Choi, "Self-supervised interactive object segmentation through a singulation-and-grasping approach," in *Proc. Eur. Conf. Comput. Vis.*, 2022, pp. 621–637.
- [7] Z. Wu, Z. Wang, Z. Wei, Y. Wei, and H. Yan, "Smart explorer: Recognizing objects in dense clutter via interactive exploration," in *Proc. IEEE/RSJ Int. Conf. Intell. Robots Syst.*, 2022, pp. 6600–6607.
- [8] M. Sundermeyer, A. Mousavian, R. Triebel, and D. Fox, "Contact-graspnet: Efficient 6-dof grasp generation in cluttered scenes," in *Proc. IEEE Int. Conf. Robot. Automat.*, 2021, pp. 13 438–13 444.
- [9] A. Murali, A. Mousavian, C. Eppner, C. Paxton, and D. Fox, "6-dof grasping for target-driven object manipulation in clutter," in *Proc. IEEE Int. Conf. Robot. Automat.*, 2020, pp. 6232–6238.
- [10] A. Goyal, A. Mousavian, C. Paxton, Y.-W. Chao, B. Okorn, J. Deng, and D. Fox, "Ifor: Iterative flow minimization for robotic object rearrangement," in *Proc. IEEE Conf. Comput. Vis. Pattern Recognit.*, 2022, pp. 14 787–14 797.
- [11] S. Noh, R. Kang, T. Kim, S. Back, S. Bak, and K. Lee, "Learning to place unseen objects stably using a large-scale simulation," *IEEE Robot. Automat. Lett.*, 2024.
- [12] G. Lin, A. Milan, C. Shen, and I. Reid, "Refinenet: Multi-path refinement networks for high-resolution semantic segmentation," in *Proc. IEEE Conf. Comput. Vis. Pattern Recognit.*, 2017, pp. 1925–1934.
- [13] Y. Yuan, J. Xie, X. Chen, and J. Wang, "Segfix: Model-agnostic boundary refinement for segmentation," in *Proc. Eur. Conf. Comput. Vis.*, 2020, pp. 489–506.
- [14] H. K. Cheng, J. Chung, Y.-W. Tai, and C.-K. Tang, "Cascadepsp: Toward class-agnostic and very high-resolution segmentation via global and local refinement," in *Proc. IEEE Conf. Comput. Vis. Pattern Recognit.*, 2020, pp. 8890–8899.
- [15] C. Tang, H. Chen, X. Li, J. Li, Z. Zhang, and X. Hu, "Look closer to segment better: Boundary patch refinement for instance segmentation," in *Proc. IEEE Conf. Comput. Vis. Pattern Recognit.*, 2021, pp. 13 926–13 935.
- [16] C. Xie, A. Mousavian, Y. Xiang, and D. Fox, "Rice: Refining instance masks in cluttered environments with graph neural networks," in *Proc. Conf. Robot Learn.*, 2022, pp. 1655–1665.
- [17] P. F. Felzenszwalb and D. P. Huttenlocher, "Efficient graph-based image segmentation," *Int. J. Comput. Vis.*, vol. 59, no. 2, pp. 167–181, 2004.
- [18] A. Richtsfeld, T. Mörwald, J. Prankl, M. Zillich, and M. Vincze, "Segmentation of unknown objects in indoor environments," in *Proc. IEEE/RSJ Int. Conf. Intell. Robots Syst.*, 2012, pp. 4791–4796.
- [19] S. Koo, D. Lee, and D.-S. Kwon, "Unsupervised object individuation from rgb-d image sequences," in *Proc. IEEE/RSJ Int. Conf. Intell. Robots Syst.*, 2014, pp. 4450–4457.
- [20] Y. Lu, Y. Chen, N. Ruozzi, and Y. Xiang, "Mean shift mask transformer for unseen object instance segmentation," *arXiv:2211.11679*, 2022.
- [21] M. Suchi, T. Patten, D. Fischinger, and M. Vincze, "Easylab: A semi-automatic pixel-wise object annotation tool for creating robotic rgb-d datasets," in *Proc. IEEE Int. Conf. Robot. Automat.* IEEE, 2019, pp. 6678–6684.
- [22] E. P. Örnek, A. K. Krishnan, S. Gayaka, C.-H. Kuo, A. Sen, N. Navab, and F. Tombari, "Supergb-d: Zero-shot instance segmentation in cluttered indoor environments," *IEEE Robot. Automat. Lett.*, 2023.
- [23] P. Krähenbühl and V. Koltun, "Efficient inference in fully connected crfs with gaussian edge potentials," *Proc. Adv. Neural Inf. Process. Syst.*, vol. 24, 2011.
- [24] L.-C. Chen, G. Papandreou, I. Kokkinos, K. Murphy, and A. L. Yuille, "DeepLab: Semantic image segmentation with deep convolutional nets, atrous convolution, and fully connected crfs," *IEEE Trans. Pattern Anal. Mach. Intell.*, vol. 40, no. 4, pp. 834–848, 2017.
- [25] L. Zhang, S. Zhang, X. Yang, H. Qiao, and Z. Liu, "Unseen object instance segmentation with fully test-time rgb-d embeddings adaptation," in *Proc. IEEE Int. Conf. Robot. Automat.* IEEE, 2023, pp. 4945–4952.
- [26] Q. M. Rahman, P. Corke, and F. Dayoub, "Run-time monitoring of machine learning for robotic perception: A survey of emerging trends," *IEEE Access*, vol. 9, pp. 20 067–20 075, 2021.
- [27] D. Hendrycks and K. Gimpel, "A baseline for detecting misclassified and out-of-distribution examples in neural networks," *arXiv preprint arXiv:1610.02136*, 2016.
- [28] Y. Gal and Z. Ghahramani, "Dropout as a bayesian approximation: Representing model uncertainty in deep learning," in *international conference on machine learning*. PMLR, 2016, pp. 1050–1059.
- [29] Y. Xia, Y. Zhang, F. Liu, W. Shen, and A. L. Yuille, "Synthesize then compare: Detecting failures and anomalies for semantic segmentation," in *Proc. Eur. Conf. Comput. Vis.*, 2020, pp. 145–161.
- [30] Q. M. Rahman, N. Sünderhauf, P. Corke, and F. Dayoub, "Fsnet: A failure detection framework for semantic segmentation," *IEEE Robot. Automat. Lett.*, vol. 7, no. 2, pp. 3030–3037, 2022.
- [31] G. Di Biase, H. Blum, R. Siegwart, and C. Cadena, "Pixel-wise anomaly detection in complex driving scenes," in *Proc. IEEE Conf. Comput. Vis. Pattern Recognit.*, 2021, pp. 16 918–16 927.
- [32] Y. Tian, Y. Liu, G. Pang, F. Liu, Y. Chen, and G. Carneiro, "Pixel-wise energy-biased abstention learning for anomaly segmentation on complex urban driving scenes," in *Proc. Eur. Conf. Comput. Vis.*, 2022, pp. 246–263.
- [33] B. Sun, J. Xing, H. Blum, R. Siegwart, and C. Cadena, "See yourself in others: Attending multiple tasks for own failure detection," in *Proc. IEEE Int. Conf. Robot. Automat.*, 2022, pp. 8409–8416.
- [34] Y. Xie, J. Zhang, H. Lu, C. Shen, and Y. Xia, "Sesv: Accurate medical image segmentation by predicting and correcting errors," *IEEE Trans. Med. Imag.*, vol. 40, no. 1, pp. 286–296, 2020.
- [35] C. B. Kuhn, M. Hofbauer, G. Petrovic, and E. Steinbach, "Reverse error modeling for improved semantic segmentation," in *Proc. Int. Conf. Image Process.*, 2022, pp. 106–110.
- [36] J. Wang, Y. Zhao, L. Qian, X. Yu, and Y. Gao, "Ear-net: error attention refining network for retinal vessel segmentation," in *Digital Image Computing: Techniques and Applications*. IEEE, 2021, pp. 1–7.
- [37] S. Ali, F. Dayoub, and A. K. Pandey, "Learning from learned network: An introspective model for arthroscopic scene segmentation," in *Proceedings of International Conference on Information and Communication Technology for Development*. Springer, 2023, pp. 393–406.
- [38] B. Cheng, R. Girshick, P. Dollár, A. C. Berg, and A. Kirillov, "Boundary iou: Improving object-centric image segmentation evaluation," in *Proc. IEEE Conf. Comput. Vis. Pattern Recognit.*, 2021, pp. 15 334–15 342.
- [39] K. He, X. Zhang, S. Ren, and J. Sun, "Deep residual learning for image recognition," in *Proc. IEEE Conf. Comput. Vis. Pattern Recognit.*, 2016, pp. 770–778.
- [40] B. Cheng, M. D. Collins, Y. Zhu, T. Liu, T. S. Huang, H. Adam, and L.-C. Chen, "Panoptic-deeplab: A simple, strong, and fast baseline for

- bottom-up panoptic segmentation,” in *Proc. IEEE Conf. Comput. Vis. Pattern Recognit.*, 2020, pp. 12475–12485.
- [41] A. G. Howard, M. Zhu, B. Chen, D. Kalenichenko, W. Wang, T. Weyand, M. Andreetto, and H. Adam, “Mobilenets: Efficient convolutional neural networks for mobile vision applications,” *arXiv:1704.04861*, 2017.
- [42] J. J. Tompson, A. Jain, Y. LeCun, and C. Bregler, “Joint training of a convolutional network and a graphical model for human pose estimation,” *Proc. Adv. Neural Inf. Process. Syst.*, vol. 27, 2014.
- [43] G. Papandreou, T. Zhu, L.-C. Chen, S. Gidaris, J. Tompson, and K. Murphy, “Personlab: Person pose estimation and instance segmentation with a bottom-up, part-based, geometric embedding model,” in *Proc. Eur. Conf. Comput. Vis.*, 2018, pp. 269–286.
- [44] D. P. Kingma and J. Ba, “Adam: A method for stochastic optimization,” *arXiv preprint arXiv:1412.6980*, 2014.
- [45] W. Liu, D. Anguelov, D. Erhan, C. Szegedy, S. Reed, C.-Y. Fu, and A. C. Berg, “Ssd: Single shot multibox detector,” in *Proc. Eur. Conf. Comput. Vis.*, 2016, pp. 21–37.
- [46] S. Zakharov, B. Planche, Z. Wu, A. Hutter, H. Kosch, and S. Ilic, “Keep it unreal: Bridging the realism gap for 2.5 d recognition with geometry priors only,” in *Proc. Int. Conf. on 3D Vision.*, 2018, pp. 1–11.
- [47] M. Shi, J. Shen, Q. Yi, J. Weng, Z. Huang, A. Luo, and Y. Zhou, “Lmffnet: A well-balanced lightweight network for fast and accurate semantic segmentation,” *IEEE Trans. Neural Netw. Learn. Sys.*, 2022.
- [48] J. Deng, W. Dong, R. Socher, L.-J. Li, K. Li, and L. Fei-Fei, “Imagenet: A large-scale hierarchical image database,” in *Proc. IEEE Conf. Comput. Vis. Pattern Recognit.*, 2009, pp. 248–255.
- [49] P. Ochs, J. Malik, and T. Brox, “Segmentation of moving objects by long term video analysis,” *IEEE Trans. Pattern Anal. Mach. Intell.*, vol. 36, no. 6, pp. 1187–1200, 2013.
- [50] J. Wang, K. Sun, T. Cheng, B. Jiang, C. Deng, Y. Zhao, D. Liu, Y. Mu, M. Tan, X. Wang *et al.*, “Deep high-resolution representation learning for visual recognition,” *IEEE Trans. Pattern Anal. Machine Intell.*, vol. 43, no. 10, pp. 3349–3364, 2020.
- [51] H. Zhao, J. Shi, X. Qi, X. Wang, and J. Jia, “Pyramid scene parsing network,” in *Proc. IEEE Conf. Comput. Vis. Pattern Recognit.*, 2017, pp. 2881–2890.
- [52] X. Zhou, R. Girdhar, A. Joulin, P. Krähenbühl, and I. Misra, “Detecting twenty-thousand classes using image-level supervision,” in *Proc. Eur. Conf. Comput. Vis.*, 2022.
- [53] M. Oquab, T. Darcet, T. Moutakanni, H. Vo, M. Szafraniec, V. Khalidov, P. Fernandez, D. Haziza, F. Massa, A. El-Nouby *et al.*, “Dinov2: Learning robust visual features without supervision,” *arXiv preprint arXiv:2304.07193*, 2023.